

RESEARCH ARTICLE

[View Article Online](#)  
[View Journal](#) | [View Issue](#)



Cite this: *Mater. Chem. Front.*,  
2022, 6, 748

## A *meta*-linkage strategy towards high-performance hosts for efficient blue thermally activated delayed fluorescence OLEDs<sup>†</sup>

Xiao-Dong Tao,<sup>abc</sup> Zhuangzhuang Wei,<sup>acd</sup> Lingyi Meng,<sup>id</sup><sup>acd</sup> Xu-Lin Chen,<sup>\*ace</sup>  
Mingxue Yang,<sup>a</sup> Yan-Yun Jing,<sup>ab</sup> Dong-Hai Zhang<sup>abc</sup> and Can-Zhong Lu<sup>id</sup><sup>\*abc</sup>

The development of high-performance host materials for blue thermally activated delayed fluorescence (TADF) emitters is crucial for realizing efficient blue organic light-emitting diodes (OLEDs). Herein, two star-shaped host materials, tris(3-(diphenylphosphanyl oxide)phenyl)phosphane oxide (**m4PO**) and tris(3-(carbazole)phenyl)phosphane oxide (**m3CzPO**), containing a triphenylphosphine oxide (TPPO) core and three *meta*-substituted diphenylphosphine oxide or carbazolyl groups, are designed and synthesized. The comparative study reveals that the *meta*-linkage strategy significantly improves the performances of the hosts. The two hosts show superhigh triplet energies of over 3.1 eV, along with high thermal stability, good carrier-transporting capability, and high film quality, which establish the basis for being potentially ideal hosts for blue TADF emitters. Based on a conventional blue TADF emitter bis[4-(9,9-dimethyl-9,10-dihydroacridine)phenyl]sulfone (DMAC-DPS), the blue TADF-OLEDs realize high performances with maximum external quantum efficiencies (EQEs) beyond 20%, maximum power efficiencies (PEs) over 40 lm W<sup>-1</sup>, a low turn-on voltage of 2.8 V, and a high luminance of up to 5170 nits.

Received 27th December 2021,  
Accepted 25th January 2022

DOI: 10.1039/d1qm01660a

[rsc.li/frontiers-materials](http://rsc.li/frontiers-materials)

## Introduction

Phosphorescent and thermally activated delayed fluorescence (TADF) emitters have attracted extensive research attention as they can achieve a theoretical internal quantum efficiency (IQE) of unity in organic light-emitting diodes (OLEDs) by utilizing both singlet and triplet excitons for light emission.<sup>1–5</sup> To suppress exciton annihilation and concentration quenching in emitting layers, generally, these triplet-excited-state-involved emitters have to be doped into suitable host materials.<sup>6–11</sup> The triplet energy of the host must be higher than that of the emitter to ensure efficient exothermic energy transfer from the host to

the guest molecule and to confine the triplet excitons within the emitting layers.<sup>12–14</sup> In the case of blue emitters, the lowest triplet state ( $T_1$ ) energy level of the host should be at least 2.9 eV.<sup>15–17</sup> To obtain high triplet energy for a host material, the molecular conjugation must be restricted, and also, the formation of intermolecular excitation such as excimers should be avoided.<sup>9,18,19</sup> These requirements make the design of host materials for triplet-excited-state-involved blue emitters particularly challenging since lowering the conjugation and reducing intermolecular interactions may negatively affect the charge transport properties, which in turn results in inferior device performance.

Much effort has been made to design host materials with high triplet energy and desired charge transport properties for blue emitters.<sup>20–28</sup> However, host materials with a  $T_1$  energy of over 3.0 eV, which are highly desired to construct deep-blue OLEDs, are still rare.<sup>29</sup> The common hosts include hole-transport-type (p-type) hosts, electron-transport-type (n-type) hosts and bipolar transport hosts. The carbazole-derived groups, which possess rigid molecular structures and good hole-transporting abilities, are popular as the building blocks for p-type and bipolar host materials.<sup>30–32</sup> However, the  $T_1$  energy level of the carbazole-based host material is usually confined by the conjugation length of carbazole fragments and the formation of excimers from adjacent carbazole units in solid states. Owing to the high  $T_1$  energies and appropriate electron-transporting ability,

<sup>a</sup> CAS Key Laboratory of Design and Assembly of Functional Nanostructures, Fujian Provincial Key Laboratory of Nanomaterials, Fujian Institute of Research on the Structure of Matter, Chinese Academy of Sciences, Fuzhou, Fujian 350002, China. E-mail: czlu@fjirs.ac.cn, xlchem@fjirs.ac.cn

<sup>b</sup> University of Chinese Academy of Sciences, Beijing 100049, China

<sup>c</sup> Xiamen Key Laboratory of Rare Earth Photoelectric Functional Materials, Xiamen Institute of Rare Earth Materials, Haixi Institutes, Chinese Academy of Sciences, Xiamen, Fujian 361021, P. R. China

<sup>d</sup> College of Chemistry and Materials Science, Fujian Normal University, Fuzhou, Fujian 350007, P. R. China

<sup>e</sup> Fujian Science & Technology Innovation Laboratory for Optoelectronic Information of China, Fuzhou, Fujian 350108, P. R. China

<sup>†</sup> Electronic supplementary information (ESI) available. CCDC 2117193. For ESI and crystallographic data in CIF or other electronic format see DOI: 10.1039/d1qm01660a

phosphine oxide derivatives were applied successfully to construct n-type and bipolar host materials for blue OLEDs.<sup>32–40</sup> Furthermore, the linkage mode of the functional groups, which influence the molecular configuration and molecular packing, is equally important in determining the properties of the host materials.<sup>41–43</sup> The influence of positional isomerism on electronic decoupling and the steric hindrance has been widely investigated.<sup>44,45</sup> *Para*-linkage generally allows planarization, which results in extended  $\pi$ -conjugation and low triplet energy.<sup>30</sup> Compared with the *para*-linkage, the *meta*-linkage leads to a lower degree of  $\pi$ -conjugation since the *meta*-positions are known to reveal the lower electron densities.<sup>43,46,47</sup> Moreover, the *meta*-linkage could lead to a more twisted molecular configuration and increased steric hindrance which are conducive to inhibiting the formation of excimers.<sup>48,49</sup> Many host materials have been designed using *meta*-linking mode for high-performance blue and white OLEDs.<sup>24,43–47</sup>

In this work, we designed two star-shaped host materials, namely tris(3-(diphenylphosphanyl oxide)phenyl)phosphane oxide (**m4PO**) and tris(3-(carbazole)phenyl)phosphane oxide (**m3CzPO**), based on a triphenylphosphine oxide (TPPO) scaffold, and three *meta*-substituted phenylphosphine oxide or carbazole fragments (Fig. 1). Tris(4-(diphenylphosphanyl oxide)phenyl)phosphane oxide (**p4PO**) containing *para*-substituted phenylphosphine

oxide units was synthesized as a reference compound for comparative study. **m4PO** and **m3CzPO** show high thermal stability, effective carrier transporting capability, and very high triplet energies of 3.18 eV and 3.10 eV, respectively, which ensures that they are suitable hosts for blue TADF emitters. The corresponding bis[4-(9,9-dimethyl-9,10-dihydroacridine)phenyl] sulfone (DMAC-DPS)-based blue TADF-OLEDs achieved high performance with the maximum external quantum efficiency (EQE) of over 20%, low turn-on voltage at *ca* 2.8 V, and a high luminance of up to 5170 nits. The result turned out better than that of the reference device based on the host **p4PO** and is comparable with the high-performance DMAC-DPS-based devices reported (summarized in Table S5, ESI<sup>†</sup>).

## Results and discussion

### Synthesis and characterization

The synthetic routes of **m4PO**, **m3CzPO**, and **p4PO** are outlined in Scheme 1. The details are described in the ESI.<sup>†</sup> The materials were fully purified by column chromatography and then by temperature-gradient vacuum sublimation, and the structures were characterized by mass spectrometry, elemental analysis, NMR spectroscopy. Single crystals of **m3CzPO** were obtained by diffusion of *n*-hexane into its  $\text{CH}_2\text{Cl}_2$  solution. However, we have failed in our deliberate attempts to crystallize the phosphine oxide host **m4PO**. Single-crystal X-ray diffraction analysis for **m3CzPO** was performed to investigate the molecular conformation and packing modes (Fig. 1), which would have a significant influence on the photophysical properties. As shown in the Fig. 1, **m3CzPO** takes a quasi-symmetric and highly twisted molecular configuration. The central TPPO scaffold adopts a pyramidal geometry with three C–P–C angles at 105.1°, 107.1°, and 107.4°, respectively. The *meta*-substituted carbazole moieties are twisted against the phenyl planes of the TPPO scaffold, with dihedral angles of 44.0°, 53.3°, and 39.9°, respectively. The single crystal packing diagram suggests that the highly twisted molecules of **m3CzPO** stack into loosely packed aggregates with

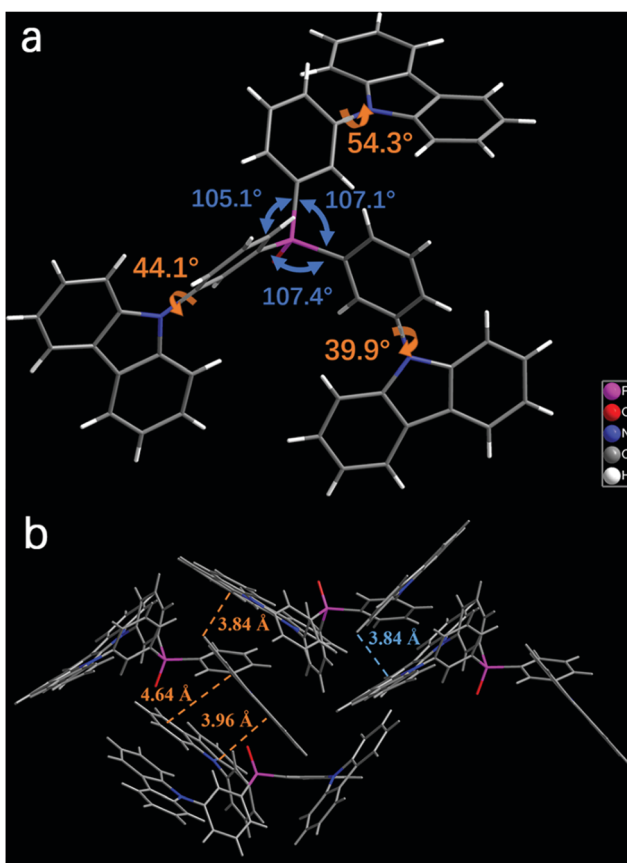
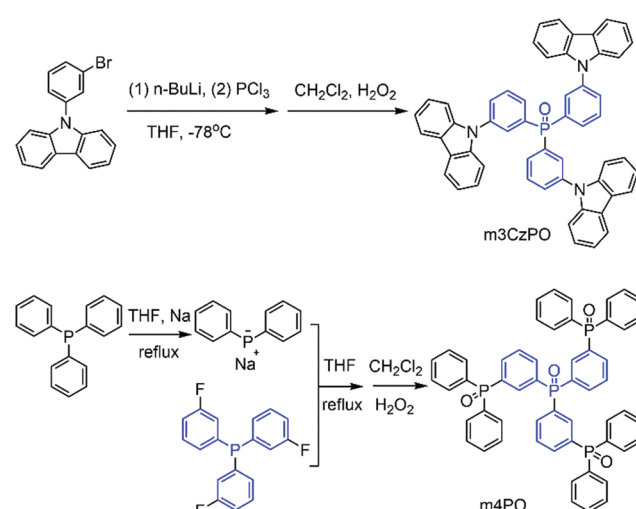


Fig. 1 (a) Crystal structure, and (b) single-crystal packing diagram of **m3CzPO**.



Scheme 1 Synthetic routes of the investigated compounds.

intermolecular distances of at least 3.84 Å, indicating no obvious intermolecular interactions. The twisted molecular configuration and the lack of intermolecular contact prevent this host material from forming excimers and exciplexes, and thus maintain high triplet energy in the solid states.

### Thermal, morphological, and electrochemical properties

The thermal properties of these host materials were investigated using thermal gravimetric analysis (TGA) and differential scanning calorimetry (DSC) measurements under a nitrogen atmosphere, and the obtained results are summarized in Table 1 and the ESI† (Fig. S1). **m4PO** and **m3CzPO** display excellent thermal stabilities with decomposition temperatures ( $T_d$ , corresponding to 5% weight loss) of 497 °C and 533 °C, and glass transition temperatures ( $T_g$ ) of 78 °C and 148 °C, respectively, which are higher than those of the reference compound **p4PO** ( $T_d$  = 492 °C,  $T_g$  not observed). Obviously, either adopting *meta*-linkage or incorporating rigid carbazole groups could improve thermal stability. The atomic force microscopy (AFM) images of vacuum-deposited neat films of **m4PO** and **m3CzPO** show uniform and smooth surfaces (Fig. S2, ESI†) with a root-mean-square (RMS) roughness of 0.413 nm and 0.465 nm, indicating the good film-forming properties of these compounds as hosts. In comparison, the neat film of **p4PO** presents a slightly rougher surface with an  $R_{\text{RMS}}$  value of 0.544 nm. The electrochemical properties of these compounds were examined by performing cyclic voltammetry (CV) in dichloromethane solutions, as shown in Fig. 2. The highest occupied molecular orbital (HOMO) levels of **m4PO** and **m3CzPO** were determined from their oxidation potentials<sup>50,51</sup> to be −6.39 eV and −5.97 eV, respectively. Compared with **m4PO**, **m3CzPO** exhibits a much shallower HOMO level owing to the replacement of the electron-deficient diphenylphosphine oxide units with the electron-donating carbazole units. The lowest unoccupied molecular orbital (LUMO) levels of **m4PO** and **m3CzPO** are −2.54 eV and −2.51 eV, respectively, evaluated from the reduction potentials. The energy levels of frontier orbitals rationalize the difference in the inherent carrier transporting capability of these compounds and the luminance of the device hosted by them.

### Theoretical simulations

The frontier molecular orbitals and electronic states of **m4PO** and **m3CzPO** have been investigated by density functional theory (DFT) and time-dependent DFT (TD-DFT) calculations at the PBE/6-311G(d,p) level.<sup>52</sup> The ground-state molecular geometries of both compounds were highly twisted after optimization. The DFT calculation results show that the HOMO

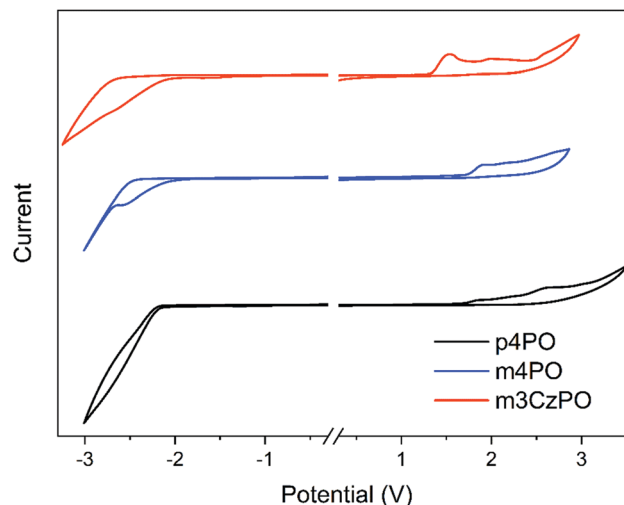


Fig. 2 Cyclic voltammogram of **p4PO**, **m4PO** and **m3CzPO** measured in  $\text{CH}_2\text{Cl}_2$  at 300 K (scanning rate: 100  $\text{mV s}^{-1}$ ).

and the LUMO of **m4PO** are distributed mostly over one of the peripheral diphenylphosphine oxide groups and the central TPPO unit, respectively (Fig. 3). The small HOMO-LUMO overlaps are uncommon for unipolar molecules containing only  $\text{P}=\text{O}$  units, which is attributed to the highly twisted geometry. For the hybrid host **m3CzPO**, as expected, the LUMO is predominantly located on the central TPPO unit, while the HOMO is largely distributed over the carbazole groups and to a lesser extent over the phenyl rings of the central TPPO unit (Fig. 3). The spatially well-separated frontier orbitals indicate its potential of ambipolar characteristics. **m3CzPO** shows a LUMO level close to that of **m4PO**, while the HOMO level of **m3CzPO** is much shallower than that of **m4PO**, which is in accordance with the CV results discussed above. As revealed by TD-DFT calculations (Fig. 3 and Fig. S13, Table S3, ESI†), the primary contribution of the lowest singlet excited state ( $S_1$ ) of each compound involves the charge transfer (CT) transition from HOMO to LUMO whereas, the  $T_1$  states of both compounds don't show predominant CT characteristics: the  $T_1$  of **m3CzPO** is a predominant locally excited ( $^3\text{LE}$ ) state, and that of **m4PO** is a hybrid state of  $^3\text{CT}$  and  $^3\text{LE}$ .

### Photophysical properties

The absorption and photoluminescence (PL) spectra of **p4PO**, **m4PO**, **m3CzPO**, and the typical blue TADF emitter DMAC-DPS in dilute dichloromethane are shown in Fig. 4a and Fig. S11 (ESI†). The UV absorption edge of **m4PO** is around 286 nm,

Table 1 Summary of properties of **p4PO**, **m4PO** and **m3CzPO**

Compound	$\lambda_{\text{PL}}^a$ [nm]	HOMO <sup>b</sup> [eV]	LUMO <sup>b</sup> [eV]	$S_1^c$ [eV]	$T_1^d$ [eV]	$T_g/T_d$ [°C]	$\mu_{\text{h}}/\mu_{\text{e}}^e$ [ $\times 10^{-6} \text{ cm}^2 \text{ V}^{-1} \text{ s}^{-1}$ ]
<b>p4PO</b>	370, 420	−6.25	−2.45	4.08	2.95	—/492	1.43/6.62
<b>m4PO</b>	292, 364	−6.39	−2.54	4.18	3.18	78/497	3.02/11.6
<b>m3CzPO</b>	396	−5.97	−2.51	3.87	3.10	148/533	13.4/4.23

<sup>a</sup> Measured in  $\text{CH}_2\text{Cl}_2$  ( $10^{-6} \text{ mol L}^{-1}$ ). <sup>b</sup> Calculated according to the CV measurements. <sup>c</sup> Estimated from the onsets of the time-resolved fluorescence spectra taken at 77 K. <sup>d</sup> Estimated from the onsets of the time-resolved phosphorescence spectra taken at 77 K. <sup>e</sup> Calculated by the SCLC method using the current density–voltage curves of single-carrier devices.

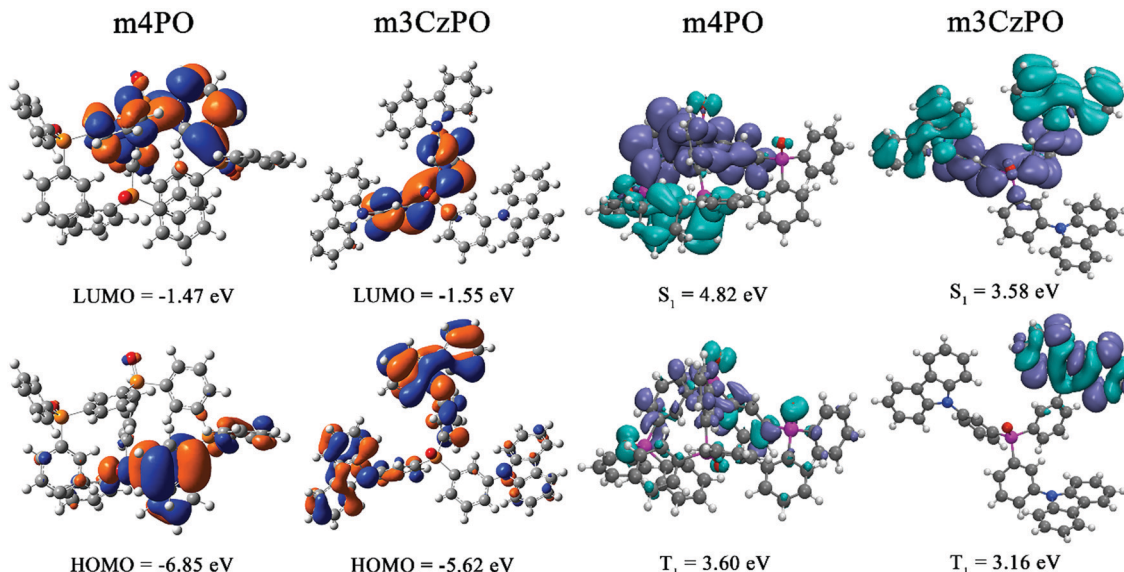


Fig. 3 Left: Frontier molecular orbital distributions, and right: energy-levels and electron-density distribution of the excited states of **m4PO** and **m3CzPO** (the purple area denotes an increase in charge density, while the blue area denotes a decrease in charge density).

which is slightly blue-shifted from that of **p4PO** (291 nm), owing to the weaker conjugation of the *meta*-linked host

(**m4PO**) compared with that of its *para*-linked counterpart (**p4PO**). By contrast, the hybrid host **m3CzPO** shows a

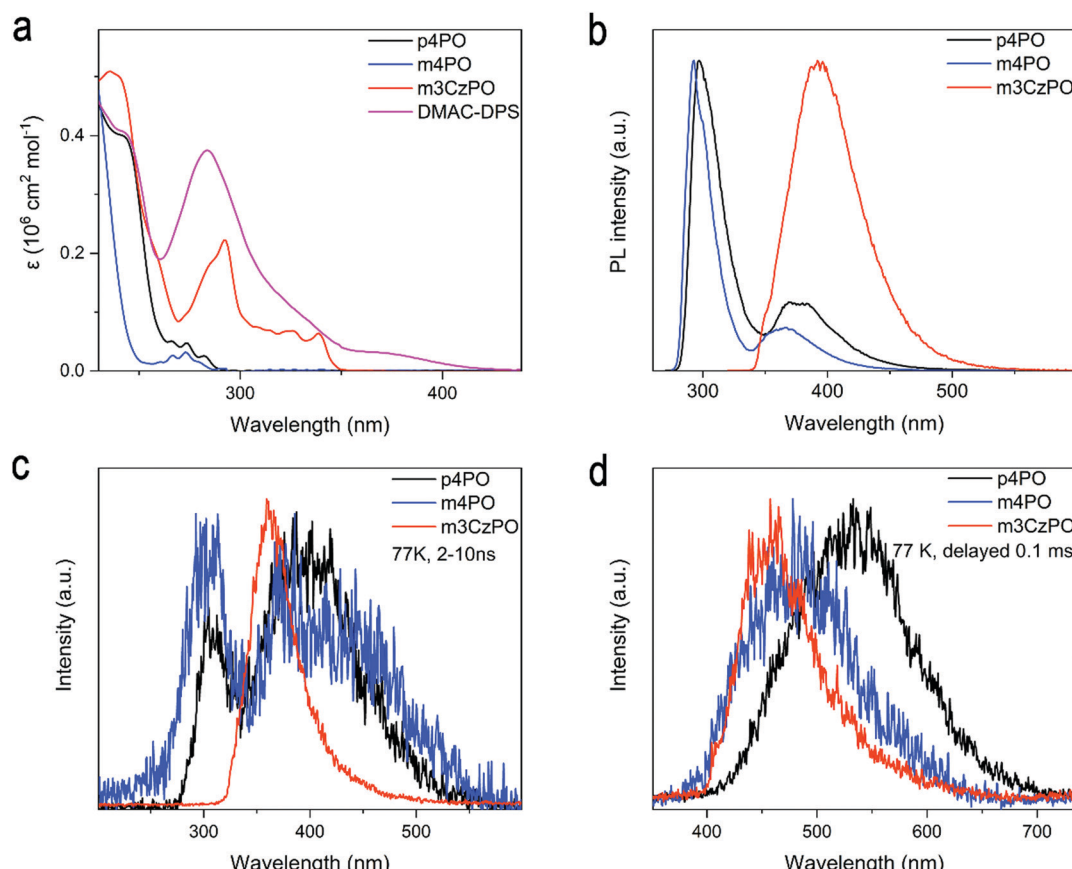


Fig. 4 (a) Absorption spectra recorded in dichloromethane ( $1.0 \times 10^{-6}$  M) at room temperature; (b) photoluminescence spectra recorded in transient PL decay of **p4PO**, **m4PO** and **m3CzPO** in dichloromethane ( $1.0 \times 10^{-6}$  M) at room temperature; (c) time-resolved fluorescence spectra (2–10 ns) in dilute 2-methyltetrahydrofuran ( $1.0 \times 10^{-6}$  M) at 77 K; and (d) time-resolved phosphorescence spectra (delayed 0.1 ms) in 2-methyltetrahydrofuran ( $1.0 \times 10^{-6}$  M) at 77 K.

significantly redshifted absorption edge (348 nm). The absorption bands of **m3CzPO** at 270–350 nm should probably originate from the  $\pi$ – $\pi^*$  and  $n$ – $\pi^*$  transitions of carbazole units. Both PL spectra of **p4PO** and **m4PO** in dilute dichloromethane recorded at 298 K comprise dual bands with similar profiles (Fig. 4b). The dual bands of the **m4PO** peak at 292 nm and 364 nm, which are slightly blue-shifted relative to those of **p4PO** (297 nm and 370 nm), respectively. Emission lifetimes of the low-energy band **m4PO** and **p4PO** were measured as 3.84 ns and 1.29 ns, respectively (Fig. S8, ESI<sup>†</sup>). Therefore, the two-band emission of the two phosphine oxide hosts could be attributed to the radiative transition from the  $S_1$  state which possesses hybrid locally excited (LE) and charge transfer (CT) characteristics. In comparison, the hybrid host **m3CzPO** exhibits a broad and structureless PL spectrum peak at 400 nm in dichloromethane, indicating its significant intramolecular charge transfer (ICT) characteristics. The PL spectra of these hosts exhibited significant spectral overlaps with the absorption spectrum of DMAC-DPS, which satisfies the basic criterion for efficient Förster resonance energy transfer (FRET) from hosts to DMAC-DPS in doped films. To evaluate the energy levels of  $S_1$  and  $T_1$  states, time-resolved fluorescence and phosphorescence spectra (Fig. 4c and d) of these host materials in 2-methyltetrahydrofuran were recorded at 77 K, from which the  $S_1$  and  $T_1$  energies were evaluated to be 4.08 eV and 2.95 eV for **p4PO**, 4.18 eV and 3.18 eV for **m4PO**, and 3.87 eV and 3.10 eV for **m3CzPO**, respectively. As expected, the  $T_1$  energy level of **m3CzPO** is very close to that of carbazole (3.11 eV, Fig. S7, ESI<sup>†</sup>), indicating effective  $\pi$ -conjugation disruption between the *meta*-substituted carbazole units and the phosphine oxide unit. Moreover, **m4PO** shows a much higher  $T_1$  energy level than that of **p4PO**, probably due to the lower  $\pi$ -conjugation induced by the *meta*-linkage. Such high  $S_1$  and  $T_1$  energies of **m4PO** and **m3CzPO** could support efficient exothermic singlet and triplet energy transfer to the blue TADF emitters.

While evaluating the feasibility of using these compounds as hosts for blue TADF emitters, DMAC-DPS ( $S_1/T_1 \approx 2.90$  eV)<sup>3</sup> was used as the guest and doped into **p4PO**, **m4PO**, and **m3CzPO** with a doping concentration of 30 wt%, respectively. The three doped films exhibit similar blue emission originated from DMAC-DPS (peaked at 473–475 nm), without emission from the host materials observed (Fig. S9, ESI<sup>†</sup>). In addition, these doped films show high photoluminescence quantum yields (PLQYs) ranging from 86% to 89%. These behaviors confirm efficient host-dopant energy transfer. However, the 30 wt% DMAC-DPS doped **m4PO** film and **m3CzPO** film reveal the shortened delayed fluorescence (DF) lifetimes, which are expectedly beneficial to quenching the suppression in the emitting layer.

### OLED characteristics

To experimentally evaluate the intrinsic carrier transporting abilities of these host materials, hole-only and electron-only devices with device structures of ITO/MoO<sub>3</sub> (6 nm)/HOST (100 nm)/MoO<sub>3</sub> (6 nm)/Al (100 nm) and ITO/LiF (1 nm)/HOST (100 nm)/LiF (1 nm)/Al (100 nm) were fabricated, in which MoO<sub>3</sub> and LiF served as hole and electron injecting layers, respectively. It is assumed that only single carriers are injected

and transported in the devices due to the work function of MoO<sub>3</sub> (or LiF) being high (or low) enough to block electron (or hole) injection. The current density *versus* voltage curves of these single-carrier devices is depicted in Fig. S14 (ESI<sup>†</sup>). The hole and electron mobilities ( $\mu_h$  and  $\mu_e$ ) of the investigated materials were determined using the space charge-limited current (SCLC) method (Table 1). Due to the electron-deficient characteristics of the P=O unit, both **p4PO** and **m4PO** expectedly reveal predominant electron-transporting properties. **m4PO** displays higher  $\mu_e$  and  $\mu_h$  mobilities ( $\mu_e = 1.16 \times 10^{-5} \text{ cm}^2 \text{ V}^{-1} \text{ S}^{-1}$  and  $\mu_h = 3.02 \times 10^{-6} \text{ cm}^2 \text{ V}^{-1} \text{ S}^{-1}$ ) than those of **p4PO** ( $\mu_e = 6.62 \times 10^{-6} \text{ cm}^2 \text{ V}^{-1} \text{ S}^{-1}$  and  $\mu_h = 1.43 \times 10^{-6} \text{ cm}^2 \text{ V}^{-1} \text{ S}^{-1}$ ), implying enhanced charge-transport capability with *meta*-linked P=O units. The carbazole/phosphine oxide hybrid host **m3CzPO** exhibits a much stronger hole transporting ability than those of **p4PO** and **m4PO**, with mobility of up to  $1.34 \times 10^{-5} \text{ cm}^2 \text{ V}^{-1} \text{ S}^{-1}$ . In addition, **m4PO** and **m3CzPO** possess a more balanced carrier transporting capability than **p4PO**.

To investigate and compare the performance of **p4PO**, **m4PO**, and **m3CzPO** as hosts in the blue OLEDs, the devices with configurations of ITO/MoO<sub>3</sub> (6 nm)/NPB (70 nm)/mCP (10 nm)/HOST: DMAC-DPS (30 wt%, 30 nm)/HOST (10 nm)/BPhen (40 nm)/LiF (1 nm)/Al (100 nm) were prepared, wherein MoO<sub>3</sub>, NPB, mCP, DMAC-DPS, BPhen, and LiF were used as the hole-injecting material, hole-transporting material, electron-blocking material, blue emitter, electron-transporting material, and electron-injecting material, respectively. The chemical structures and energy levels of the materials used in these devices are illustrated in Fig. 5a and Fig. S12 (ESI<sup>†</sup>).

The graphic and numerical data of device performance are shown in Fig. 5b–d and Table 2, respectively. All three devices exhibit typical blue electroluminescence (EL) from DMAC-DPS with the spectral peaks at 470–473 nm and the Commission Internationale de l'Eclairage (CIE) coordinates of (0.16, 0.24), indicating efficient host-to-dopant energy transfer and the good confinement of emissive excitons on the blue emitter. Meanwhile, all devices exhibit approximately equal turn-on voltages of around 2.8 V, indicating a low injection barrier for both electrons and holes to enter the emitting layer.

The OLED hosted by **p4PO** shows a maximum EQE of 16.9%, a maximum current efficiency (CE) of  $30.8 \text{ cd A}^{-1}$ , a maximum power efficiency (PE) of  $35.8 \text{ lm W}^{-1}$ . In comparison, the **m4PO**-hosted and **m3CzPO**-hosted devices revealed significantly increased efficiencies, with maximum EQEs of 20.5% and 20.7%, CEs of  $36.2 \text{ cd A}^{-1}$  and  $36.6 \text{ cd A}^{-1}$ , and PEs of  $40.6 \text{ lm W}^{-1}$  and  $40.7 \text{ lm W}^{-1}$ , respectively. Moreover, the maximum luminances of the **m4PO**-hosted and **m3CzPO**-hosted OLEDs reach 3804 and 5170  $\text{cd m}^{-2}$ , which are much higher than that of the **p4PO**-hosted device ( $2780 \text{ cd m}^{-2}$ ). The improved EL efficiencies and luminance could be mainly ascribed to more efficient and balanced carrier transport and exciton confinement of the hosts with the *meta*-linkage strategy.

For further comparison, two conventional p-type hosts, 4,4'-bis(*N*-carbazolyl)-1,1'-biphenyl (CBP) and 3,3'-di(9H-carbazol-9-yl)-1,1'-biphenyl (mCBP), were employed to fabricate OLEDs

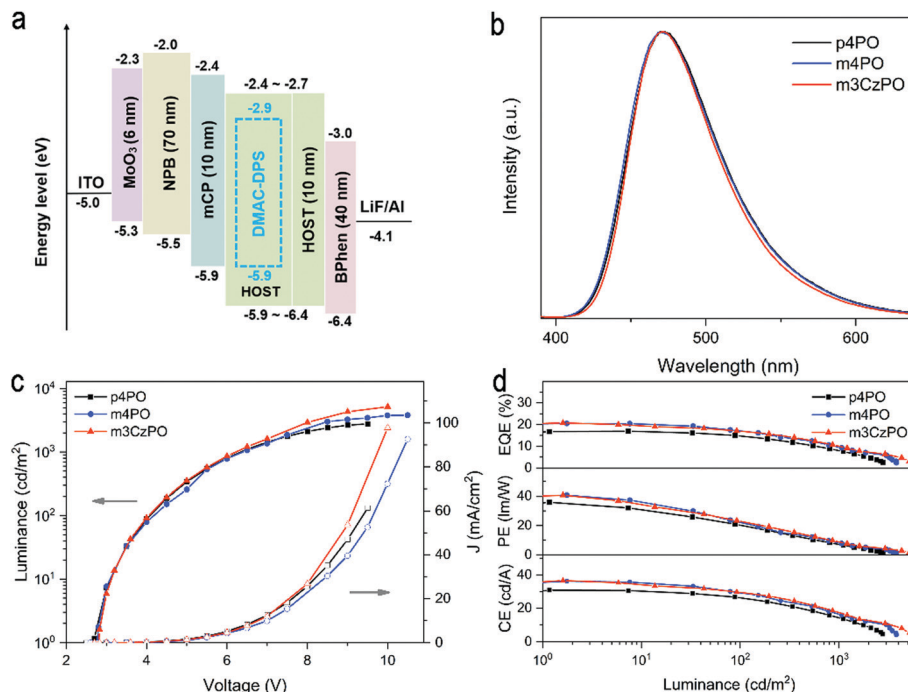


Fig. 5 (a) Energy level diagram of the OLEDs; (b) electroluminescence (EL) spectrum; (c) current density–luminance–voltage ( $J$ – $V$ – $L$ ) characteristics; and (d) external quantum efficiency (EQE), power efficiency (PE) and current efficiency (CE) versus luminance characteristics.

Table 2 EL performance of OLEDs using DMAc-DPS as the emitter, and **p4PO**, **m4PO** and **m3CzPO** as the host matrix

Host	Emitter	$\lambda_{EL}^a$ [nm]	$L_{max}^b$ [cd m <sup>-2</sup> ]	$V^c$ [V]	$CE_{max}$ [cd A <sup>-1</sup> ]	$PE_{max}$ [lm W <sup>-1</sup> ]	EQE <sub>max</sub> [%]	CIE <sup>d</sup>
<b>p4PO</b>	DMAC-DPS	470	2780	2.7	30.8	35.8	16.9	(0.16, 0.24)
<b>m4PO</b>	DMAC-DPS	473	3804	2.8	36.2	40.6	20.5	(0.16, 0.24)
<b>m3CzPO</b>	DMAC-DPS	471	5170	2.8	36.6	40.6	20.7	(0.16, 0.24)

<sup>a</sup> EL maximum wavelength at 6 V. <sup>b</sup> The maximum luminance. <sup>c</sup> Turn-on voltage taken at 1 cd m<sup>-2</sup>. <sup>d</sup> Value at 500 cd m<sup>-2</sup>.

with the same configuration of ITO/MoO<sub>3</sub> (6 nm)/NPB (70 nm)/mCP (10 nm)/CBP or mCBP: DMAc-DPS (30 wt%, 30 nm)/**m4PO** (10 nm)/BPhen (40 nm)/LiF (1 nm)/Al (100 nm). As shown in Fig. S22 and Table S4 (ESI<sup>†</sup>), the device performance of the CBP-hosted device (EQE<sub>max</sub> of 6.2%) and the mCBP-hosted device (EQE<sub>max</sub> of 15.8%) are inferior to those of **m4PO**-hosted and **m3CzPO**-hosted devices. This can be attributed to the relatively low triplet energies of CBP ( $T_1 = 2.6$  eV) and mCBP ( $T_1 = 2.9$  eV),<sup>53</sup> which may result in back energy transfer from the dopant (DMAc-DPS,  $T_1 = 2.91$  eV) to the host.

## Conclusions

In summary, two new host materials, **m4PO** and **m3CzPO**, have been constructed with a TPPO scaffold and three *meta*-substituting diphenylphosphine oxide units or carbazole units. The *meta*-linkage between the diphenylphosphine oxide or carbazole substituents and the TPPO scaffold could bring in the highly twisted molecular conformation, in turn leading to a minimized  $\pi$  conjugation and high  $T_1$  energies of 3.18 eV for **m4PO** and 3.10 eV for **m3CzPO**, respectively. Compared with the *para*-linking

counterpart **p4PO**, compounds **m4PO** and **m3CzPO** exhibit higher  $T_1$  energy levels, improved thermal stability, and enhanced and balanced carrier transporting capability. By using DMAc-DPS as the blue TADF emitter, the multilayer OLEDs hosted by **m4PO** and **m3CzPO** achieved maximum EQEs of 20.5% and 20.7%, CE of 36.2 cd A<sup>-1</sup> and 36.6 cd A<sup>-1</sup>, PE of 40.6 lm W<sup>-1</sup> and 40.6 lm W<sup>-1</sup>, and maximum luminescence of 3804 cd m<sup>-2</sup> and 5170 cd m<sup>-2</sup> respectively, which were significantly increased in contrast to the **p4PO**-based reference device. This work exemplifies the superiority of the *meta*-linkage strategy for the development of blue host materials.

## Conflicts of interest

There are no conflicts to declare.

## Acknowledgements

This work was supported by the Strategic Priority Research Program of the Chinese Academy of Sciences (XDB20000000),

the Key Research Program of Frontier Science, CAS (QYZDJ-SSW-SLH033), the National Natural Science Foundation of China (52073286, 21805281, 21875252, 21773246, and 21403176), the Natural Science Foundation of Fujian Province (2006L2005, 2019J01125, and 2019J01123), the Fujian Science & Technology Innovation Laboratory for Optoelectronic Information of China (2021ZR132), the Youth Innovation Foundation of Xiamen City (3502Z20206082, and 3502Z20206083), and the Opening Project of PCOSS, Xiamen University (202014).

## References

- 1 M. A. Baldo, D. F. O'Brien, Y. You, A. Shoustikov, S. Sibley, M. E. Thompson and S. R. Forrest, Highly efficient phosphorescent emission from organic electroluminescent devices, *Nature*, 1998, **395**, 151–154.
- 2 C. Y. Chan, L. Y. Cui, J. U. Kim, H. Nakanotani and C. Adachi, Rational molecular design for deep-blue thermally activated delayed fluorescence emitters, *Adv. Funct. Mater.*, 2018, **28**, 1706023.
- 3 B. L. Q. Zhang, S. Huang, H. Nomura, H. Tanaka and C. Adachi, Efficient blue organic light-emitting diodes employing thermally activated delayed fluorescence, *Nat. Photonics*, 2014, **8**, 326–332.
- 4 J. U. Kim, I. S. Park, C. Y. Chan, M. Tanaka, Y. Tsuchiya, H. Nakanotani and C. Adachi, Nanosecond-time-scale delayed fluorescence molecule for deep-blue OLEDs with small efficiency rolloff, *Nat. Commun.*, 2020, **11**, 1–8.
- 5 X. Cai, D. Chen, K. Gao, L. Gan, Q. Yin, Z. Qiao, Z. Chen, X. Jiang and S.-J. Su, “Trade-Off” hidden in condensed state solvation: multiradiative channels design for highly efficient solution-processed purely organic electroluminescence at high brightness, *Adv. Funct. Mater.*, 2018, **28**, 1704927.
- 6 A. Ligthart, X. d. Vries, L. Zhang, M. C. Pols, P. A. Bobbert, H. v. Eersel and R. Coehoorn, Effect of triplet confinement on triplet–triplet annihilation in organic phosphorescent host–guest systems, *Adv. Funct. Mater.*, 2018, **28**, 1804618.
- 7 S. Scholz, D. Kondakov, B. Lussem and K. Leo, Degradation mechanisms and reactions in organic light-emitting devices, *Chem. Rev.*, 2015, **115**, 8449–8503.
- 8 P. Chen, Y. Bai, M. Q. Lyu, J. H. Jun, M. M. Hao and L. Z. Wang, Progress and perspective in low-dimensional metal halide perovskites for optoelectronic applications, *Sol. RRL*, 2018, **2**, 1700186.
- 9 C. H. Chen, W. C. Ding, B. Y. Lin, J. J. Huang, M. K. Leung, J. H. Lee and T. L. Chiu, Long-distance triplet diffusion and well-packing hosts with ultralow dopant concentration for achieving high-efficiency TADF OLED, *Adv. Opt. Mater.*, 2021, **9**, 2100857.
- 10 W. X. Song, Q. H. Xu, J. N. Zhu, Y. Chen, H. C. Mu, J. H. Huang and J. H. Su, Imidazo 1,2-*b* pyridazine as building blocks for host materials for high-performance red-phosphorescent organic light-emitting devices, *ACS Appl. Mater. Interfaces*, 2020, **12**, 19701–19709.
- 11 M. A. Bazrafshan, M. Ansari-Rad and S. H. Pilehrood, Effect of energetic disorder on triplet-triplet annihilation in organic semiconductors, *Phys. Rev. B*, 2020, **101**, 094204.
- 12 X. Yang, G. Zhou and W. Y. Wong, Functionalization of phosphorescent emitters and their host materials by main-group elements for phosphorescent organic light-emitting devices, *Chem. Soc. Rev.*, 2015, **44**, 8484–8575.
- 13 M. Godumala, S. Choi, M. J. Cho and D. H. Choi, Thermally activated delayed fluorescence blue dopants and hosts: from the design strategy to organic light-emitting diode applications, *J. Mater. Chem. C*, 2016, **4**, 11355–11381.
- 14 L. M. Chen, I. H. Lin, Y. C. You, W. C. Wei, M. J. Tsai, W. Y. Hung and K. T. Wong, Substitution effect on carbazole-centered donors for tuning exciplex systems as cohost for highly efficient yellow and red OLEDs, *Mater. Chem. Front.*, 2021, **5**, 5044–5054.
- 15 H. W. Chen, J. H. Lee, B. Y. Lin, S. Chen and S. T. Wu, Liquid crystal display and organic light-emitting diode display: present status and future perspectives, *Light: Sci. Appl.*, 2018, **7**, 17168.
- 16 S. Kappaun, C. Slugovc and E. J. List, Phosphorescent organic light-emitting devices: working principle and iridium based emitter materials, *Int. J. Mol. Sci.*, 2008, **9**, 1527–1547.
- 17 Y. X. Wang, J. H. Yun, L. Wang and J. Y. Lee, High triplet energy hosts for blue organic light-emitting diodes, *Adv. Funct. Mater.*, 2020, **31**, 2008332.
- 18 C. M. Han, J. Zhang, P. Ma, W. B. Yang and H. Xu, Host engineering based on multiple phosphorylation for efficient blue and white TADF organic light-emitting diodes, *Chem. Eng. J.*, 2021, **405**, 126986.
- 19 D. L. Li, J. Y. Li, D. Liu, W. Li, C. L. Ko, W. Y. Hung and C. H. Duan, Highly efficient simple-structure sky-blue organic light-emitting diode using a bicarbazole/cyanopyridine bipolar host, *ACS Appl. Mater. Interfaces*, 2021, **13**, 13459–13469.
- 20 Y. Lu, D. D. Zhang, J. B. Wei, Z. Y. Liu, C. Zhang, Y. W. Zhang, X. Li, H. Lee, J. H. Kwon, X. W. Wang and L. Duan, Bee-shaped host with ideal polarity and energy levels for high-efficiency blue and white fluorescent organic light-emitting diodes, *Chem. Eng. J.*, 2021, **411**, 128457.
- 21 D. L. Li, D. Liu, J. Y. Li, R. Z. Dong, B. T. Liu and Q. H. Wei, Low-driving-voltage sky-blue phosphorescent organic light-emitting diodes with bicarbazole–bipyridine bipolar host materials, *Mater. Chem. Front.*, 2021, **5**, 2867–2876.
- 22 H. H. Li, Y. Tao, Y. B. Zhi, R. F. Chen, H. Li, G. C. Xing, S. Xu and W. Huang, Evoking non-bonding S–pi interaction by aryl phosphine sulfide for selectively enhanced electronic property of organic semiconductors, *Chem. Eng. J.*, 2020, **380**, 122562.
- 23 L. Ding, S. Du, L. S. Cui, F. H. Zhang and L. S. Liao, Novel spiro-based host materials for application in blue and white phosphorescent organic light-emitting diodes, *Org. Electron.*, 2016, **37**, 108–114.
- 24 Q. Wang, F. Lucas, C. Quinton, Y. K. Qu, J. Rault-Berthelot, O. Jeannin, S. Y. Yang, F. C. Kong, S. Kumar, L. S. Liao, C. Poriel and Z. Q. Jiang, Evolution of pure hydrocarbon hosts: simpler structure, higher performance and universal application in RGB phosphorescent organic light-emitting diodes, *Chem. Sci.*, 2020, **11**, 4887–4894.

25 H. Huang, X. Yang, B. Pan, L. Wang, J. S. Chen, D. G. Ma and C. L. Yang, Benzimidazole–carbazole-based bipolar hosts for high efficiency blue and white electrophosphorescence applications, *J. Mater. Chem.*, 2012, **22**, 13223.

26 N. Q. Li, D. Y. Chai, Z. X. Chen, C. J. Zhou, F. Ni, Z. Y. Huang, X. S. Cao, G. H. Xie, K. Li and C. L. Yang, Molecular engineering by  $\sigma$ -Bond spacer enables solution-processable host materials for TADF emitter towards high-performance OLEDs, *Chem. Eng. J.*, 2020, **396**, 125276.

27 X. Tang, X. Y. Liu, Y. Yuan, Y. J. Wang, H. C. Li, Z. Q. Jiang and L. S. Liao, High-efficiency white organic light-emitting diodes integrating gradient exciplex allocation system and novel *d*-spiro-*a* materials, *ACS Appl. Mater. Interfaces*, 2018, **10**, 29840–29847.

28 W. C. Chen, Y. Yuan, Z. L. Zhu, Z. Q. Jiang, S. J. Su, L. S. Liao and C. S. Lee, De novo design of *d*-Sigma-*A* molecules as universal hosts for monochrome and white phosphorescent organic light-emitting diodes, *Chem. Sci.*, 2018, **9**, 4062–4070.

29 Y. X. Wang, J. H. Yun, L. Wang and J. Y. Lee, High triplet energy hosts for blue organic light-emitting diodes, *Adv. Funct. Mater.*, 2020, **31**, 2008332.

30 C. M. Han, W. B. Yang and H. Xu, Asymmetrically phosphorylated carbazole host for highly efficient blue and white thermally activated delayed fluorescence diodes, *Chem. Eng. J.*, 2020, **401**, 126049.

31 H. H. Chou and C. H. Cheng, A highly efficient universal bipolar host for blue, green, and red phosphorescent OLEDs, *Adv. Mater.*, 2010, **22**, 2468–2471.

32 J. S. Wang, C. F. Jiang, C. Liu, H. Y. Liu and C. Yao, Highly efficient blue, orange and red PhOLEDs with low roll-off of efficiency using a carbazole dendritic thermally activated delayed fluorescence (TADF) material as host, *Mater. Lett.*, 2018, **233**, 149–152.

33 H. F. Li, M. Hong, A. Scarpaci, X. Y. He, C. Risko, J. S. Sears, S. Barlow, P. Winget, S. R. Marder, D. Kim and J. L. Brédas, Chemical stabilities of the lowest triplet state in aryl sulfones and aryl phosphine oxides relevant to oled applications, *Chem. Mater.*, 2019, **31**, 1507–1519.

34 D. X. Ding, Z. Zhang, Y. Wei, P. F. Yan and H. Xu, Spatially optimized quaternary phosphine oxide host materials for high-efficiency blue phosphorescence and thermally activated delayed fluorescence organic light-emitting diodes, *J. Mater. Chem. C*, 2015, **3**, 11385–11396.

35 K. Duan, D. Wang, M. Yang, Z. Liu, C. Wang, T. Tsuboi, C. Deng and Q. Zhang, Weakly conjugated phosphine oxide hosts for efficient blue thermally activated delayed fluorescence organic light-emitting diodes, *ACS Appl. Mater. Interfaces*, 2020, **12**, 30591–30599.

36 J. Q. Ding, Q. Wang, L. Zhao, D. G. Ma, L. X. Wang, X. B. Jing and F. S. Wang, Design of star-shaped molecular architectures based on carbazole and phosphine oxide moieties: towards amorphous bipolar hosts with high triplet energy for efficient blue electrophosphorescent devices, *J. Mater. Chem.*, 2010, **20**, 8126–8133.

37 J. U. Kim, M. Y. Wong, S. Kumar, O. G. Hayes, F. Duncan, C. Y. Chan, Y. W. Wong, H. Ye, L. S. Cui, H. Nakanotani, E. Zysman-Colman and C. Adachi, High-triplet-energy bipolar host materials based on phosphine oxide derivatives for efficient sky-blue thermally activated delayed fluorescence organic light-emitting diodes with reduced roll-off, *Chem. Lett.*, 2019, **48**, 1225–1228.

38 J. Zhang, D. Ding, Y. Wei, F. Han, H. Xu and W. Huang, Multiporphine-oxide hosts for ultralow-voltage-driven true-blue thermally activated delayed fluorescence diodes with external quantum efficiency beyond 20, *Adv. Mater.*, 2016, **28**, 479–485.

39 H. Yang, Q. Liang, C. Han, J. Zhang and H. Xu, A phosphanthrene oxide host with close sphere packing for ultralow-voltage-driven efficient blue thermally activated delayed fluorescence diodes, *Adv. Mater.*, 2017, **29**, 1700553.

40 J. Zhang, C. M. Han, F. S. Du, C. B. Duan, Y. Wei and H. Xu, High-power-efficiency white thermally activated delayed fluorescence diodes based on selectively optimized intermolecular interactions, *Adv. Funct. Mater.*, 2020, **30**, 2005165.

41 S. Y. Byeon, J. H. Kim and J. Y. Lee, CN-modified host materials for improved efficiency and lifetime in blue phosphorescent and thermally activated delayed fluorescent organic light-emitting diodes, *ACS Appl. Mater. Interfaces*, 2017, **9**, 13339–13346.

42 B. Pan, B. Wang, Y. X. Wang, P. Xu, L. Wang, J. S. Chen and D. G. Ma, A simple carbazole-*N*-benzimidazole bipolar host material for highly efficient blue and single layer white phosphorescent organic light-emitting diodes, *J. Mater. Chem. C*, 2014, **2**, 2466–2469.

43 W. X. Song, L. J. Shi, L. Gao, P. J. Hu, H. C. Mu, Z. Y. Xia, J. H. Huang and J. H. Su, 1,2,4-Triazolo 1,5-*a* pyridine as building blocks for universal host materials for high-performance red, green, blue and white phosphorescent organic light-emitting devices, *ACS Appl. Mater. Interfaces*, 2018, **10**, 5714–5722.

44 L. Sicard, C. Quinton, J. D. Peltier, D. Tondelier, B. Geffroy, U. Biapo, R. Metivier, O. Jeannin, J. Rault-Berthelot and C. Poriel, Spirobifluorene regioisomerism: a structure–property relationship study, *Chemistry*, 2017, **23**, 7719–7727.

45 C. Poriel, C. Quinton, F. Lucas, J. Rault-Berthelot, Z. Q. Jiang and O. Jeannin, Spirobifluorene dimers: understanding how the molecular assemblies drive the electronic properties, *Adv. Funct. Mater.*, 2021, **31**, 2104980.

46 X. L. Lv, B. Wang, J. H. Tan, Z. Huang, Q. Zhang, S. P. Xiang, W. Liu, S. Q. Zhuang and L. Wang, Constructing diazacarbazole–bicarbazole bipolar hybrids by optimizing the linker group for high efficiency, low roll off electrophosphorescent devices, *Dyes Pigm.*, 2017, **136**, 54–62.

47 Y. L. Zhao, C. Wu, P. L. Qiu, X. P. Li, Q. Wang, J. S. Chen and D. G. Ma, New benzimidazole-based bipolar hosts: highly efficient phosphorescent and thermally activated delayed fluorescent organic light-emitting diodes employing the same device structure, *ACS Appl. Mater. Interfaces*, 2016, **8**, 2635–2643.

48 A. Maheshwaran, V. G. Sree, H. Y. Park, H. Kim, S. H. Han, J. Y. Lee and S. H. Jin, High efficiency deep-blue phosphorescent organic light-emitting diodes with CIE  $x, y$  ( $\leq 0.15$ )

and low efficiency roll-off by employing a high triplet energy bipolar host material, *Adv. Funct. Mater.*, 2018, **28**, 1802945.

49 D. Liu, D. L. Li, M. Wang and W. Li, 1,2,4-Triazole-containing bipolar hosts for blue and green phosphorescent organic light-emitting diodes, *J. Mater. Chem. C*, 2016, **4**, 7260–7268.

50 Y. Y. Jing, X. D. Tao, M. X. Yang, X. L. Chen and C. Z. Lu, Triptycene-imbedded thermally activated delayed fluorescence emitters with excellent film morphologies for applications in efficient nondoped and doped organic light-emitting devices, *Chem. Eng. J.*, 2021, **413**, 127418.

51 X. L. Chen, X. D. Tao, Z. Z. Wei, L. Y. Meng, F. L. Lin, D. H. Zhang, Y. Y. Jing and C. Z. Lu, Thermally activated delayed fluorescence amorphous molecular materials for high-performance organic light-emitting diodes, *ACS Appl. Mater. Interfaces*, 2021, **13**(39), 46909–46918.

52 Z. Wei, S. Lin, T. Zuo, Q. Li, S. Jiang, F. Qi, M. Yang, J. Gu, L. Meng and C. Z. Lu, Thermally activated delayed fluorescence materials with aggregation-induced emission properties: a QM/MM study, *Phys. Chem. Chem. Phys.*, 2021, **23**, 25789–25796.

53 Y. Liu, C. Li, Z. Ren, S. Yan and M. R. Bryce, All-organic thermally activated delayed fluorescence materials for organic light-emitting diodes, *Nat. Rev. Mater.*, 2018, **3**, 18020.